

# 1 Deep learning models to predict flood events in fast-flowing watersheds

2 Marco Luppichini<sup>a,b,\*</sup>, Michele Barsanti<sup>c</sup>, Roberto Giannecchini<sup>b,d,e</sup>, Monica Bini<sup>b,d,f</sup>

3 <sup>a</sup>Department of Earth Sciences, University of Study of Florence, Via La Pira 4, Florence, Italy.

4 <sup>b</sup>Department of Earth Sciences, University of Pisa, Via S. Maria, 52, 56126 Pisa, Italy

5 <sup>c</sup>Department of Civil and Industrial Engineering, University of Pisa, Largo L. Lazzarino, 56122 Pisa, Italy

6 <sup>d</sup>CIRSEC Centro Interdipartimentale di Ricerca per lo Studio degli Effetti del Cambiamento Climatico dell'Università di Pisa, Via del  
7 Borghetto 80, 56124 Pisa, Italy.

8 <sup>e</sup>Institute of Geosciences and Earth Resources, IGG-CNR, via Moruzzi 1, 56124 Pisa, Italy

9 <sup>f</sup>Istituto Nazionale di Geofisica e Vulcanologia (INGV), Via Vigna Murata 605, 00143 Roma, Italy.

## 10 Abstract

11 This study aims to explore the reliability of flood warning forecasts based on deep learning models, in particular Long-Short Term  
12 Memory (LSTM) architecture. We also wish to verify the applicability of flood event predictions for a river with flood events lasting only  
13 a few hours, with the aid of hydrometric control stations. This methodology allows for the creation of a system able to identify flood  
14 events with acceptable errors within several hours' notice. In terms of errors, the results obtained in this study can be compared to those  
15 obtained by using physics-based models for the same study area. These kinds of models use few types of data, unlike physical models that  
16 require the estimation of several parameters. However, the deep learning models are data-driven and for this reason they can influence the  
17 results obtained. Therefore, we tested the stability of the models by simulating the missing or wrong input data of the model, and this  
18 allowed us to achieve excellent results. Indeed, the models were stable even if several data were missing. This method makes it possible to  
19 lay the foundations for the future application of these techniques when there is an absence of geological-hydrogeological information  
20 preventing physical modelling of the run-off process or in cases of relatively small basins, where the complex system and the  
21 unsatisfactory modelling of the phenomenon do not allow a correct application of physical-based models. The forecast of flood events is  
22 fundamental for correct and adequate territory management, in particular when significant climatic changes occur. The study area is that of  
23 the Arno River (in Tuscany, Italy), which crosses some of the most important cities of central Italy, in terms of population, cultural  
24 heritage, and socio-economic activities.

25  
26 *Keywords:* Arno River, Deep Learning, Fast Catchment Basin, Flood Forecasting, Hydraulic models, LSTM.

## 27 1. Introduction and goals

28 River flow prediction is a fundamental goal for early flood warning, water resource management, water demand assessment, irrigation,  
29 agriculture, and hydroelectric power generation. These aspects become more and more critical in the context of climate changes. The  
30 extreme weather events causing flash floods, floods, and debris flow phenomena have relevant socio-economic implications and represent  
31 a significant scientific issue producing extensive literature on the subject (e.g., Bates et al., 2008; Bryndal et al., 2017; Gaume et al., 2016,  
32 2009; IPCC, 2014).

33 The method most currently used for modelling of the hydrologic scenario simplifies the hydrologic system features to predict their  
34 behaviour (Antonetti and Zappa, 2018). The physical models aim to understand and replicate the natural events by using mathematical and  
35 numeric methods based on several parameters simplifying the natural phenomena (Jaiswal et al., 2020). However, the systems in nature  
36 (including the hydrologic ones) are inherently heterogeneous (Marçais and de Dreuzy, 2017) and physically-based models may show  
37 inherent limitations in reproducing natural phenomena (Islam, 2011). Furthermore, in a physical hydraulic model, a wrong setting or a  
38 wrong estimation of the parameters cause an increase in model errors and this is the main drawback of the physical models (Luppichini et  
39 al., 2019).

40 The recent developments of artificial intelligence (AI) and graphic processor units (GPU) have enabled advancements in deep learning  
41 applications, and innovative approaches based on multilayer artificial neural networks (ANN) (Goodfellow et al., 2016; LeCun et al.,  
42 2015). The application of deep learning models in various real-world cases, especially in the time series prediction (Fawaz et al., 2020; Yi  
43 et al., 2019; Zheng et al., 2019) has been successful. These procedures are the most appropriate to tackle the noisy and chaotic nature of  
44 the time series forecasting problems (Livieris et al., 2020). Several authors have applied different deep learning techniques to predict river  
45 flows with promising results (Boulmaiz et al., 2020; Chattopadhyay et al., 2020; Kratzert et al., 2018; Marçais and de Dreuzy, 2017; Sit et  
46 al., 2020; Tien Bui et al., 2020; Van et al., 2020). The long short-term memory (LSTM) is one of the most popular, efficient and deeply  
47 used learning techniques (Fawaz et al., 2020), widely applied in flood prediction studies (Boulmaiz et al., 2020; Hu et al., 2020; Kratzert et  
48 al., 2018; Le et al., 2019; Li et al., 2020; Liu et al., 2020; Nguyen and Bae, 2020).

49 This research aims to demonstrate that deep learning approaches can be used to predict flood events in watersheds characterized by fast  
50 flood events. The study area is represented by the Arno River basin (in Tuscany, Italy), which experienced many damaging floods in the  
51 past (Becchi I., 1986; Caporali et al., 2005) and which is characterised by very sudden events that developed in less than 24 hours. We  
52 have used very high-frequency data to reconstruct flood events in great detail. The work is designed to create deep learning models able to  
53 predict flood events within a few hours' notice. The architecture of the applied deep learning model is based on an encoder-decoder LSTM  
54 layer, by simply using rainfall and hydrometric height data. The few types of data exploited by a deep learning model, as opposed to a  
55 physical-based model, allows the user to apply the same techniques of this study to different cases. Deep learning techniques will make it  
56 possible to create flood alarm systems in catchments for which there is scarce territorial information. Many studies have applied these  
57 techniques to large river basins characterized by multi-day events. Some examples may include studies that have involved several  
58 watersheds scattered across various continents (Boulmaiz et al., 2020; Kratzert et al., 2018), large basins of North America  
59 (Chattopadhyay et al., 2020), and Chinese rivers having large flow rates (Le et al., 2019; Li et al., 2020; Liu et al., 2020; Van et al., 2020).

60 Thus, the application of the method to smaller catchments is excellent news and of relevant importance for many purposes.

Formatted: Not Highlight

Formatted: Not Highlight

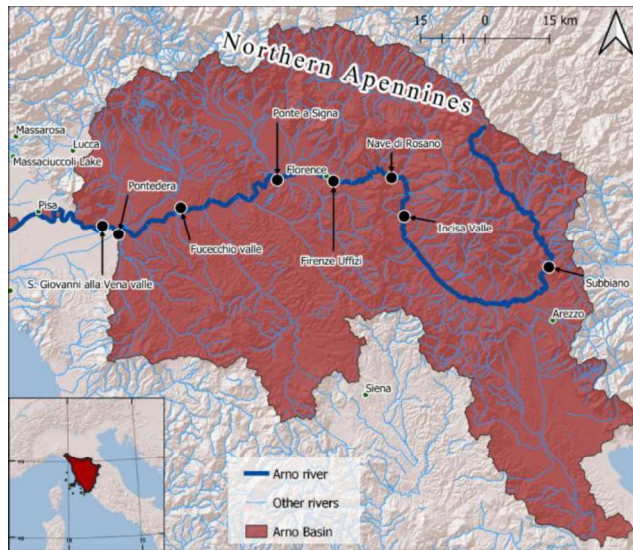
Formatted: English (United States)

## 61 2. Study Area

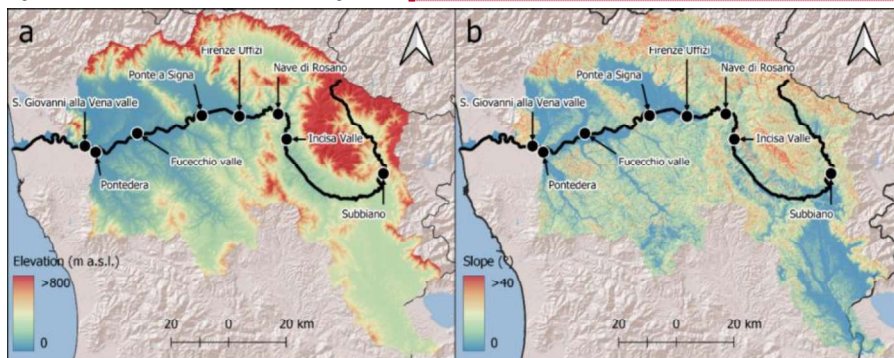
62 The study area is located in Tuscany, central Italy. The region includes many important elements at risk: high population and density  
63 (especially in fluvial plains); cultural heritage; historical towns rich in art and monuments and crossed by rivers (e.g., Florence and Pisa);  
64 industrial and artisanal settlements often situated in fluvial plains.

65 The Arno River basin (Figure 1) is approximately 8300 km<sup>2</sup> wide, the fifth in extension in Italy, and is bordered by the Apennine chain  
66 from north to east. The average and maximum elevations are about 350 and 1600 m a.s.l. respectively. The Arno is the main river in  
67 Tuscany and one of the longest (240 km) in Italy. Thus, flood forecasting is strategic in the Arno River basin, since the river crosses the

68 two main Tuscan cities of Florence and Pisa, as well as many production centers. Figure 1 also shows the location of the hydrometric  
 69 stations used in this study, whereas Figure 2a and 2b show the digital terrain model (DTM) and the slope of the basin.  
 70 Owing to its geological, geomorphological and morphometric structure, the Arno River basin is characterized by a general relatively short  
 71 run-off time. However, different sectors of the river characterized by different run-off times can be recognized: in the mountainous hilly  
 72 area, the run-off times range from 4 to 6 hours, whereas in the lowland areas the run-off time is ca 20-24 hours (Autorità di Bacino del  
 73 Fiume Arno, 1989), approximately. This behaviour is interesting to understand whether the applied methodology has limitations when the  
 74 basin run-off times are short.



75  
 76 Figure 1. The Arno River basin and its main drainage network.



77

Formatted: Normal

Formatted: Font: 10 pt

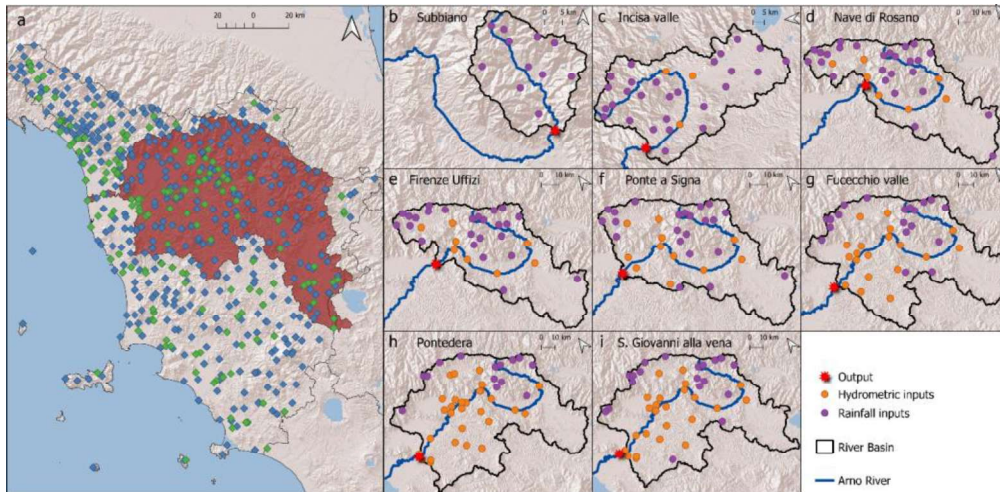
78 Figure 2. Morphological characteristics of the Arno River Basin: a) 10×10m DEM provided by the Tuscany Region  
79 (<https://www.regione.toscana.it/~geoscopio>); b) grid of the slope obtained from DEM. The black dots identify the eight hydrometric stations used  
80 in this work.

### 81 3. Methodology

#### 82 3.1. Database and data input pre-processing

83 The dataset used in this work (provided by the Regional Hydrologic Service, hereafter SIR), comes from a very rich monitoring network  
84 that includes 487 raingauges and 193 hydrometers (Figure 4Error! Reference source not found.), with a sampling time of 15 minutes.  
85 For our models, we selected the most complete time series using 48 raingauges and 35 hydrometric stations for the decade 2010-2020. The  
86 15-minute sampling time allowed us to better describe the phenomena that develop over a short time span. In fact, a low sampling  
87 frequency could lead to run-off and rainfall curves that do not adequately represent the natural phenomenon. From this point of view, deep  
88 learning models are capable of reproducing these curves, resulting to be precise but not very accurate. On the other hand, the high  
89 frequency of sampling involves an increase of the noise in the data that could create errors in the models. In our case, we have no noise  
90 signal in the data, and for this reason we have chosen to use the maximum resolution available for the study area. In our study, we want to  
91 get as close as possible to the real phenomenon by limiting simplifications in the flow or in the rainfall curves.

92



93  
94 Figure 3. a) Monitoring network of SIR (15-minute sampling frequency; source: <https://www.sir.toscana.it/consistenza-rete>). The brown region  
95 indicates the Arno River Basin closed at the hydrometric station of S. Giovanni alla Vena, whereas the blue rhombi represent the raingauges  
96 and the green rhombi represent the hydrometers. b-i) Distribution of output hydrometers (red stars), input hydrometers (orange) and raingauges  
97 (violet) in the 8 sub-basins simulated in this work.

98 For our purposes, the Arno River basin was divided into eight sub-basins closed at specific hydrometric stations, which were used as  
99 model outputs. From upstream to downstream, we selected Subbiano, Incisa valle, Nave di Rosano, Firenze Uffizi, Ponte a Signa,

100 Fucecchio valle, Pontedera and S. Giovanni alla Vena (see Figure 2). These stations were chosen for having almost complete time series  
 101 with a small number of missing values, and for being in strategic positions for monitoring of the river. The stations of Subbiano, Incisa  
 102 Valle, and Nave di Rosano are positioned upstream of the city of Florence, thus allowing to predict flood events upstream of the city of  
 103 Florence. Firenze Uffizi station is a key to understanding the hydraulic behaviour of the river in the most important and vulnerable towns  
 104 or cities of Tuscany. Ponte a Signa station is near a large flood reservoir, whereas the Fucecchio valle station provides information on the  
 105 hydraulic behaviour of the river in a completely flat area. Pontedera station is near the Scolmatore, an artificial canal built after the 1966  
 106 flood in order to protect Pisa (the second main Tuscan city crossed by the Arno River) from flooding. The Scolmatore Canal drains the  
 107 waters of the Arno River directing them towards the sea. S. Giovanni alla Vena station is the nearest one upstream to Pisa. Figure 4 shows  
 108 the hydrometric and rainfall stations used for each sub-basin model. We chose the input stations according to their datasets and to their  
 109 geographical positions. This choice was made to obtain a homogenous distribution of station in each sub-basin. Table 1 lists the  
 110 characteristics of each modelled sub-basin and the relative stations considered. For each sub-basin, Mean Annual Precipitation (MAP) and  
 111 Mean Annual Temperature (MAT) were computed by using the 1920-2020 data on the basis of the meteorological stations indicated.

112  
 113 **Table 1. Features of each modelled sub-basin and of the stations used (MAP: Mean Annual Precipitation; MAT: Mean Annual Temperature**  
 114 **(MAT) and relative standard deviation - Data from 1920 to 2020).**

Output Hydrometric Station	Sub-basin area (km <sup>2</sup> )	Sub-basin average elevation (m a.s.l.)	n. input raingauges	n. input hydrometers	MAP	MAT
Subbiano	750	750	11	0	1295 ± 276	13 ± 2
Incisa Valle	2,840	580	28	3	956 ± 193	18 ± 1
Nave di Rosano	3,840	460	26	8	1017 ± 190	17 ± 1
Firenze Uffizi	3,970	450	25	9	1014 ± 189	17 ± 1
Ponte a Signa	4,540	430	22	12	989 ± 185	18 ± 1
Fucecchio	6,600	370	19	20	997 ± 188	18 ± 1
Pontedera	7,850	340	14	30	1000 ± 188	19 ± 1
S. Giovanni alla Vena	8,030	320	19	25	996 ± 186	19 ± 1

115  
 116 For each output hydrometer, we built a deep learning model to predict its 15-minute measurements ( $H_t$ ). The mathematical expression of  
 117 the model, representative of all the investigated sub-basins, can be defined as follows:

$$\hat{H} = f(X_t) = f(H_{t-1}, H_{t-2}, \dots, H_{t-n}, R_{t-1}, R_{t-2}, \dots, R_{t-m}) \quad (1)$$

118 where  $\hat{H}$  stands for the predicted hydrometric height at time  $t$ ;  $H_{t-1}, H_{t-2}, \dots, H_{t-n}$  are the antecedent hydrometric heights (up to  $t-1, t-2, \dots, t-n$  time steps);  $R_{t-1}, R_{t-2}, \dots, R_{t-m}$  are the antecedent rainfall ( $t-1, t-2, \dots, t-m$  time steps).

120 Some tests and trials highlighted the need to create an input dataset with  $t$  up to 96 steps. To decrease the noise contained by many steps  
 121 and close measurements, we provided every  $t$  for the first previous hour and then one every 4 steps (e.g.,  $t-0, t-1, t-2, t-3, t-4, t-8, t-12, t-16, \dots, t-96$ ) up to the 24<sup>th</sup> hour.

123 The evolution of the riverbed influences the hydrometric measurements. Since a hydrometer measures the flow heights relative to a fixed  
 124 point over time, sediment deposits near the hydrometer cause the measured value to be higher than the correct value (systematic error). On  
 125 the contrary, the riverbed erosion causes a measurement lower than the correct one. For this reason, we could observe negative values of  
 126 hydrometer measures or a progressive movement of the minimum annual level of the river. Furthermore, measurement errors could occur,

Formatted: Not Strikethrough

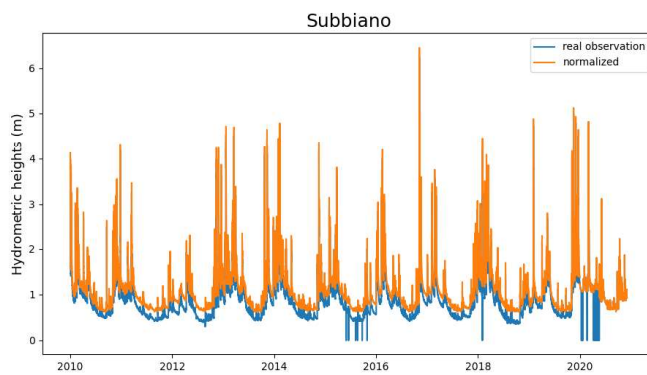
Formatted: Font: 9 pt

Formatted: Font: 9 pt

Formatted: Font: 9 pt

Formatted: Font: 9 pt

127 inducing inconsistencies and incoherence in the dataset. These problems of hydrometric measurements are summarized in Figure 4 (blue  
128 line), which shows that the past year presents the highest minimum flow of the river and that there are some errors when measurements are  
129 equal to 0. For this reason, we normalized the hydrometric measurements for each time series used by removing the incorrect data and  
130 standardizing the measurements and then comparing the minimum measured each year with the last one (Figure 4, orange lines).



131  
132 **Figure 4. Standardization of a hydrometric height time series (the example is referred to Subbiano station). We removed all fake data and**  
133 **calculated the minimum river level value that was stationary over time each year.**

### 134 3.2. Model development

135 To accomplish the deep learning models of this study, we mainly used the open-source framework Tensorflow (Abadi et al., 2015) and the  
136 libraries Numpy, Pandas, Scikit-Learn and Keras (Chollet, 2015) in Python language v 3.7 (van Rossum and Drake, 2009). The  
137 architecture of the developed models is based on an encoder-decoder LSTM, formed by two pairs of LSTM nodes (Figure 5). This  
138 architecture allows usage of an LSTM to read the input sequence, one step at a time, in order to obtain a fixed-size vector representation in  
139 a data structure that occupies a large amount of memory. We then introduce another LSTM to extract the output sequence from that vector  
140 (Sutskever et al., 2014). The encoder is composed of two sequence layers (LSTM) of 32 and 16 units, respectively, followed by a repeat  
141 vector node. The repeat vector layer repeats the incoming inputs for a specific number of times. The decoder is composed of two LSTM  
142 layers of 16 and 32 units respectively, followed by a time-distributed dense node as output of our model. To evaluate the discrepancy  
143 between the predicted and the measured values, we used a loss function for each observation, which allowed us to calculate the cost  
144 function. We needed to minimize the cost function by identifying the optimized values for each weight. Thanks to multiple iterations, the  
145 optimization algorithm computes the weights that minimize the cost function. In our implementation, we used the Adam optimizer  
146 (Kingma and Ba, 2014). Adam is an adaptive learning speed method, meaning that it computes individual learning rates for several  
147 parameters (Kingma and Ba, 2014). To stop the training, we used the specific API of Keras and, in particular, the early stopping method.  
148 This method allows the training procedure to stop when the monitored metric, namely the value of the cost function, has ceased to  
149 improve. Therefore, given all the possible hypotheses, we wanted to find the best one (called "optimal"). This hypothesis would make it  
150 possible for us to make more accurate estimates, still based on the data available. We split the dataset into three parts: training, validation,  
151 and test dataset (Figure 5). The training dataset includes the 2010-2017 data, and represents the input in the learning step. The validation  
152 dataset is composed of the 2017-2019 data and is used to calculate and optimize the loss function in the learning phase. Finally, we used



153 the test dataset (2019-2021) to evaluate the final model: the prediction step allowed us to forecast the hydrometric heights of the river  
 154 because these data are unknown to the model. This partition of 60% - 20% - 20% for training, validation and test dataset is used by several  
 155 studies (e.g., Hu et al., 2020; Li et al., 2020; Nguyen and Bae, 2020) and permits to have sufficient data for the training and the evaluation  
 156 of the model. In detail, Li et al. (2020) use a similar subdivision of the dataset considering only one year for validation and for the test  
 157 dataset.

158 The cost function used was the mean square error (MSE) calculated on the validation dataset. The partition of the whole dataset permitted  
 159 to minimize the overfitting effect on the training set. We built a model for each hydrometric station and 25 forecasting steps for a total of  
 160 200 models considering the eight sub-basins modelled. The forecasting steps are one every hour from 0 to 24 hours.

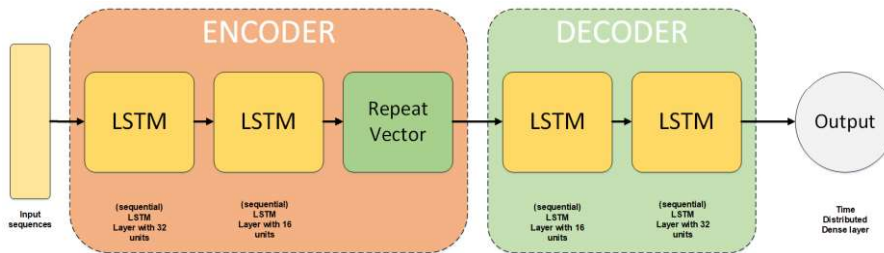
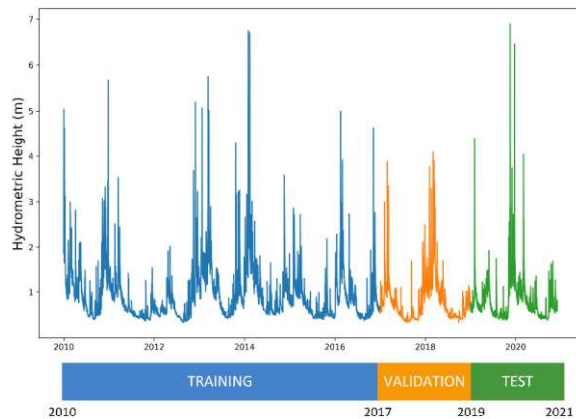


Figure 5. Architecture of the deep learning model used in this study, based on the use of the LSTM node.



163  
 164 Figure 6. Partition of the dataset in training, validation and test datasets. Training and validation datasets are the input for model training. The  
 165 test datasets predict events that are unknown to the model. The example is referred to San Giovanni alla Vena station.

#### 166 4. Results

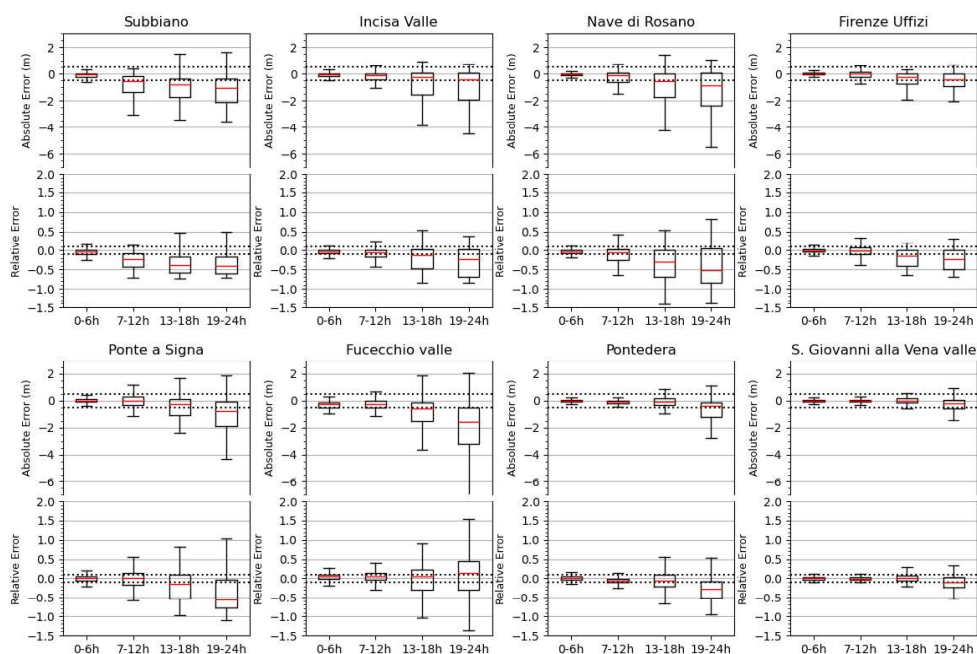
167 We evaluated the accuracy and precision of the models by analysing the model errors when predicting the maximum effects. For each  
 168 station, Figure 7 shows the prediction accuracy of the 30 highest events occurred in 2019 and 2020, highlighting the absolute error, i.e.,

Commented [m1]: Valutazione del modello

Commented [m2]: Ripartizione / Divisione

Formatted: Not Highlight

169 the difference between the predicted value and the observed value. We also computed the relative error by dividing the absolute error by  
 170 the measured value. We partitioned the results into four groups: 0-6 h, 7-12 h, 13-18 h and 19-24 h. In all cases, we can observe that the  
 171 longer the forecast time, the greater were the errors. Furthermore, the percentage errors were higher for the upstream than for the  
 172 downstream stations (Figure 7).

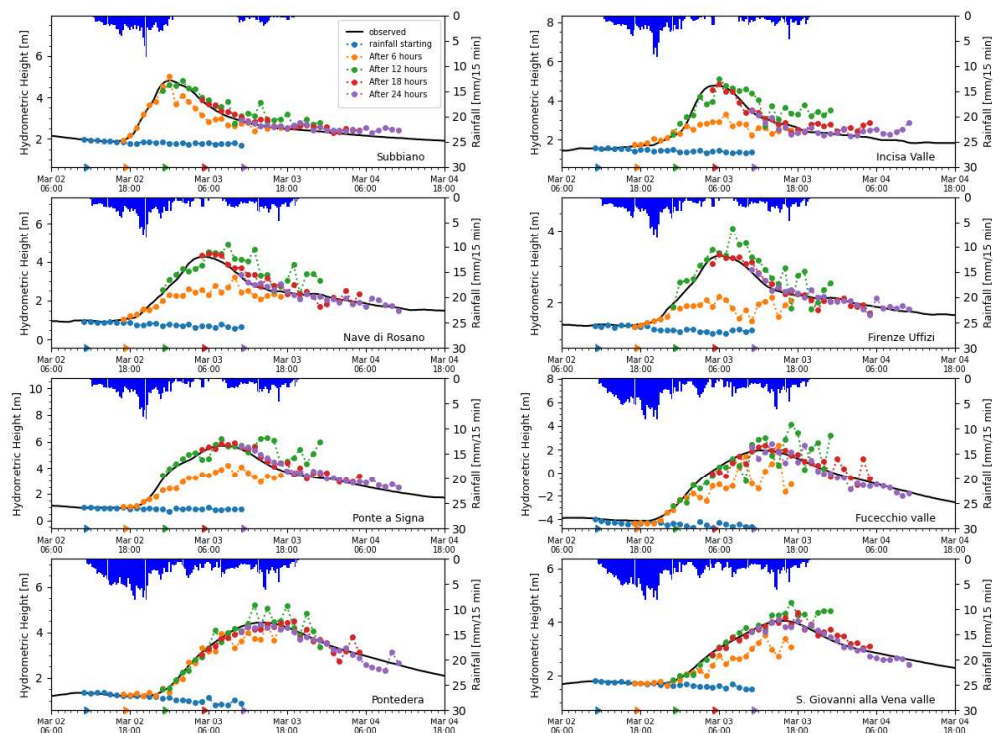


173  
 174 **Figure 7. Absolute and relative model errors for the 30 most severe events occurred between 2019 and 2020 (test dataset). In absolute error graphs,**  
 175 **the dotted lines mark the range between -0.5 and +0.5m. In relative error graphs, the dotted lines mark the range between -0.1 and +0.1. The**  
 176 **boxes represent the interval between the 25<sup>th</sup> and the 75<sup>th</sup> percentiles (Q1 and Q3). IQR is the interquartile range Q3-Q1. The upper whisker will**  
 177 **extend to the last datum lower than  $Q3 + 1.5 \cdot IQR$ . Similarly, the lower whisker will reach the first datum higher than  $Q1 - 1.5 \cdot IQR$ . The green**  
 178 **lines represent the medians.**

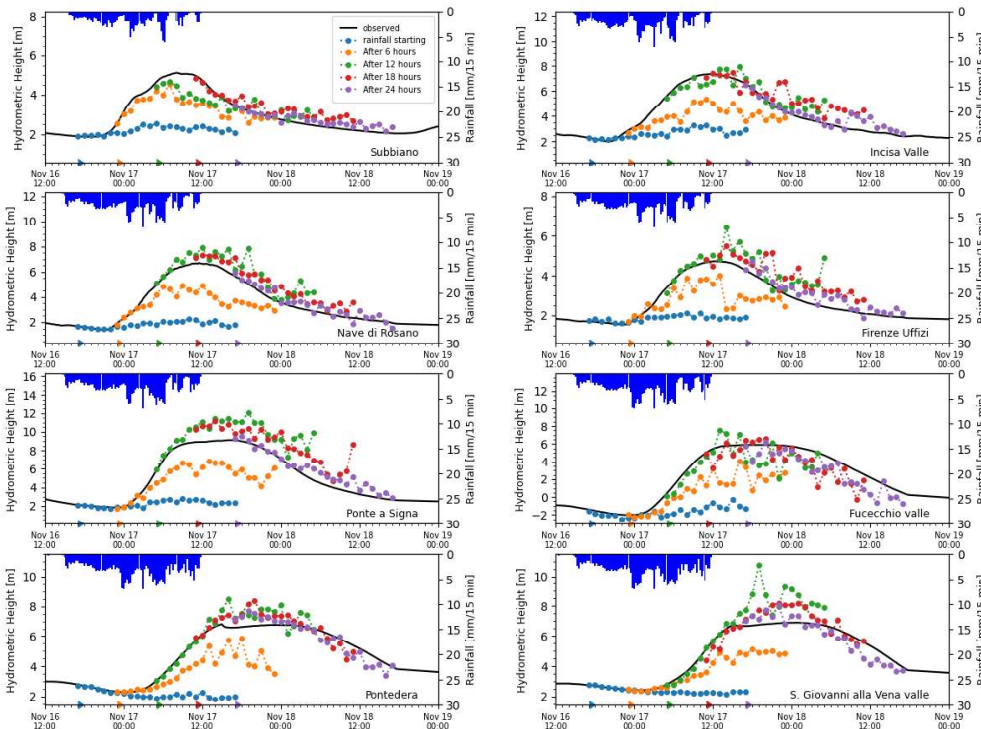
179 Figures 8 and 9 show two events that occurred on 3<sup>rd</sup> March 2020 and 17<sup>th</sup> November 2019, respectively and that represent examples of the  
 180 behaviour of the Arno River during flooding episodes. Both events triggered a flood warning and the exceeding of the alert thresholds for  
 181 the whole course of the river. Specifically, the event of 17<sup>th</sup> November 2019 is of considerable importance: in the 10-year time series used  
 182 to train the model (see Figure 6), there is only one other case similar to that of 17<sup>th</sup> November 2019 (see Figure 9). The rainfall (ca 40 mm)  
 183 fell from 2020-03-02 06:00 to 2020-03-04 00:00 on the basin of San Giovanni alla Vena. Instead, the event of 17<sup>th</sup> November 2019 was  
 184 characterized by ca 65 mm of rainfall that fell on the same basin from 2019-11-16 12:00 to 2019-11-17 12:00. For this reason, we can  
 185 consider the two cases as representative of an ordinary alert event (3<sup>rd</sup> March 2020, Figure 8) and an exceptional alert event (17<sup>th</sup>  
 186 November 2019, Figure 9).



187 The figures show a first prediction (blue line), which started when the rainfall over the entire Arno River basin began to increase. The  
 188 subsequent forecasts were temporally spaced 6 hours from each other. Each prevision lasted for 24 hours after the start. Prediction errors  
 189 mainly depend on two factors: the location of the hydrometric stations, and the time interval between the start of the forecast and the  
 190 instant of time when the level reaches its maximum value. The simulations carried out just before the onset of the rainfall event (blue line)  
 191 or before the maximum values of cumulative rainfall on the river basin are characterized by the higher errors, with an impossibility for the  
 192 model to simulate the flow event (Figures 9 and 10). The errors are lower for the simulation temporally close to the maximum flow event.  
 193 When comparing Figures 9 and 10, the errors are higher in the second case, when the hydrometric heights of the river are greater.



194  
 195 **Figure 8. Simulation of the 3<sup>rd</sup> March 2020 event, where the hydrometric level exceeded the alert threshold in all stations. The first forecast (blue**  
 196 **line) begins when the rainfall on the Arno river basin increases. Subsequent predictions are temporally spaced 6 hours one from the other, each**  
 197 **lasting 24 hours. The coloured triangles on the time axis indicate the start of each prediction. The blue bars indicate rainfall.**



198  
 199 **Figure 9.** Simulation of the 17<sup>th</sup> November 2019 severe event, where the hydrometric level exceeded the alert threshold in all stations. The first  
 200 forecast (blue line) begins when the rainfall on the Arno river basin increases. Subsequent predictions are temporally spaced 6 hours from each  
 201 other, each lasting for 24 hours. The coloured triangles on the time axis indicate the start of each prediction. The blue bars indicate rainfall.

202 **5. Discussion**

203 As a result of the high frequency of data sampling (15 minutes), we obtained a large amount of data, which allowed for efficient model  
 204 learning. Model errors are influenced by the forecasting time and by the location of the hydrometric stations. The forecasts for the  
 205 hydrometric stations located at higher mean elevation exhibit the highest errors. Prediction with more than 7-12 hours for this type of basin  
 206 is difficult, and is characterized by high errors. The problem is reasonably due to the shorter run-off time typical of these basins. The time  
 207 interval between maximum rainfall event and maximum hydrometric height is obviously variable for the analyzed stations and it  
 208 characterizes the different sub-basins. The shortest interval is associated with Subbiano (average of 13 hrs), the longest is attributable to S.  
 209 Giovanni alla Vena (average of 23 hrs). Run-off times influence the capacity of the model to achieve a good prediction of the flow events.

210 Deep learning models are the simplest ones relatively to the data to be used and they show large flexibility at different basin scales. Their  
 211 main advantage is the dynamics simplification of a run-off process by using only rainfall and hydrometric data. On the other hand,  
 212 physically-based models require large amounts of different data that are sometimes very difficult to find or do not have a sufficient  
 213 resolution and need specific assumptions. For example, a very low topographic resolution can cause a high error when applying a physical  
 214 model (Luppichini et al., 2019) so that specific surveys are necessary. The few types of data necessary to create a deep learning model  
 215 allow us to apply it in different environmental situations. These flow forecasts are valid for the entire Arno River, from its origin to the  
 216 position just before its mouth. Therefore, we think these models could be applied to watercourses with different hydraulic behaviour. For  
 217 these basins, it would be useful to compare our errors with those obtained by Ercolani and Castelli (2017) which used the hydrological  
 218 model MOBIDIC (*MOdello di Bilancio Idrologico Distribuito e Continuo*). MOBIDIC is a physically-based model used by the Tuscany  
 219 Region authorities for the analysis of flood alarms (Ercolani and Castelli, 2017). Even in the case of the physical model, errors are higher  
 220 in basins with shorter run-off times (e.g., Subbiano and Nave di Rosano stations) and they diminish for larger basins. In that specific case,  
 221 the model tends to overestimate the water flow when the warning time is several hours (greater than about 12 hours from the maximum  
 222 event) (Ercolani and Castelli, 2017). Instead, the deep learning models underestimate the hydrometric heights even with high errors when  
 223 the simulation is performed before the rain falls on the basin. These models do not provide any specific information helping to understand  
 224 when it will start raining and before this time, the rain is constantly equal to 0. Once the rainfall has started, our model can predict the  
 225 hyetograph and understand how the hydraulic regime will evolve. The rainfall onset is a critical point in a flood warning system based on  
 226 deep learning techniques. The forecast rainfall data can be made useful by implementing the classical techniques (physical models,  
 227 analysis of satellite images, etc.), which can help these models overcome the current limits of these methods.

228 The deep run-off learning models need to use all the input stations for prediction, and this could be one of the main drawbacks of these  
 229 techniques. In real conditions, one (or more) stations might not be working during a specific flood event, making a good prediction of the  
 230 future flow height impossible. In cases like those of our study area, where the monitoring network is quite dense, this drawback is  
 231 overcome by creating several models based on the use of different stations. We could apply the naivest procedure by inserting the missing  
 232 values of an unworking station with 0 mm (rainfall) or 0 m (hydrometric height). However, in theory, this procedure might introduce  
 233 greater errors in the flood events simulation, and we could test this by changing the input data of random groups of stations with values all  
 234 equal to 0, simulating the case of the missing values for the event of S. Giovanni alla Vena station. We made a simulation as if 5, 50 and  
 235 95% of the rainfall and hydrometric stations used in the model for San Giovanni alla Vena were missing. These percentages correspond to  
 236 2 non-working stations, 22 non-working stations and 42 non-working stations respectively. For each of the three tests, we simulated the  
 237 predictions from 0 to 24 hrs with a step of 1 h. We repeated these simulations 10 times changing the random group of stations each time.  
 238 We calculated these errors on the 30 highest events that occurred in 2019 and 2020 (test dataset). The 30 events used to calculate the  
 239 variations had a hydrometric height between 1.40 and 6.90 m. We computed the percentage variation as follows:

$$\text{Percentage Variation} = \frac{\bar{y}_i - y_i}{m_i} \cdot 100 \quad (1)$$

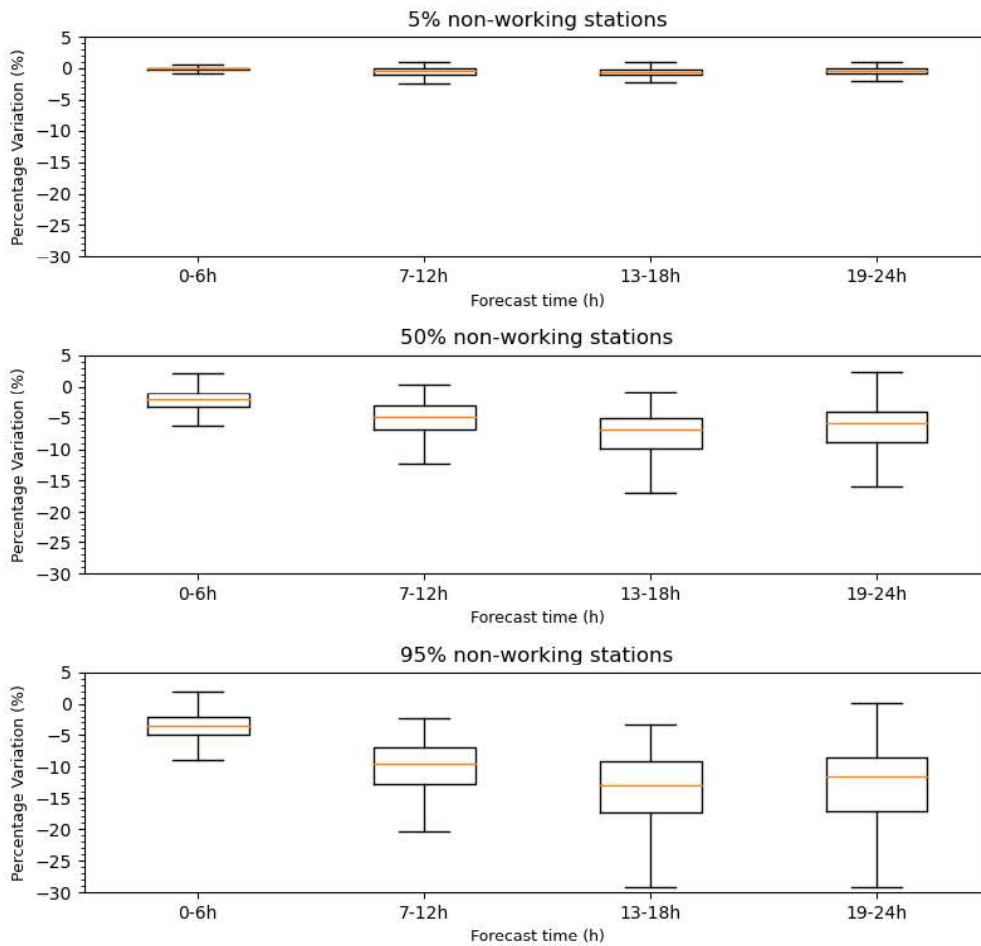
240 where  $y_i$  is the absolute error calculated on the difference between the measured hydrometric heights ( $m_i$ ) and the predicted hydrometric  
 241 heights estimated by using the real dataset;  $\bar{y}_i$  is the absolute error computed by using the dataset with the simulation of missing values.  
 242 The absolute errors ( $\bar{y}_i$  and  $y_i$ ) are calculated as follows:

$$\text{absolute error} = m_{sim} - m_{ob} \quad (2)$$

243 where  $m_{sim}$  is the result of the model and  $m_{ob}$  is the observed measure. By merging equation 1 and equation 2, we can write the  
 244 percentage variation as follows:

$$\text{Percentage Variation} = \frac{\overline{m_i^s} - m_i^s}{m_i^s} \cdot 100 \quad (3)$$

245 where  $\overline{m_i^s}$  is the result of the model with the dataset modified with the missing value and  $m_i^s$  is the result of the model with the original  
246 dataset. A reduction in percentage variation indicates a greater underestimation of the flow level compared to models with the data  
247 available. The percentage variation is influenced by the number of non-working stations (Figure 10). With 5% of non-working stations, the  
248 model errors increase by less than 5% for each time of prediction. A 5% underestimation corresponds to a variation of the estimated  
249 hydrometric height of about 0.07 – 0.35 m. When the number of non-working stations is 95%, the model errors increase with an  
250 underestimation of the flow level that varies with the forecast time. The worst cases are for the greater forecast times with errors even  
251 higher than 20% (Figure 10). A variation of 20% corresponds to a variation of the estimated hydrometric height of about 0.28 – 1.48 m.  
252 This test allows us to observe how models can experience small increases in error when the number of non-working stations is small, but  
253 also that these errors increase greatly when the number of non-functioning stations increases significantly. In physical models, a  
254 precipitation estimate can be given by one group of stations rather than another, with results that in most cases are not significantly  
255 different. In deep learning models, which are data-driven, each station acquires greater importance and its correct management and  
256 maintenance have a greater influence on the final results of the models. For the applicability of these models in alert systems for territorial  
257 management bodies, proper maintenance and management of the monitoring stations are necessary for correct flow modeling.



258  
 259 Figure 10. Percentage variation in the absolute error estimate of the San Giovanni alla Vena station if we consider the 30 most serious events of  
 260 2019 and 2020 by simulating a variable number of non-working stations. The box indicates the range between the 25<sup>th</sup> and 75<sup>th</sup> percentiles (Q1 and  
 261 Q3). IQR is the Q3-Q1 interquartile range. The upper whisker will extend to the last data lower than  $Q3 + 1.5 \cdot IQR$ . Likewise, the lower whisker  
 262 will reach the first datum greater than  $Q1 - 1.5 \cdot IQR$ . The orange lines represent the medians.

263 **6. Conclusion**

264 This study demonstrates that deep learning tools can be a viable alternative to physically-based models for the forecast of flood events in  
265 basins characterized by short run-off times. The study developed deep learning models based on the LSTM network for the Arno River,  
266 one of the most important and critical Italian rivers, by using eight hydrometric stations. Unlike physically-based models, these approaches  
267 offer the advantage of using only few types of data. This feature reduces model influences resulting from the accessibility of required  
268 information, which for some watersheds can be very difficult to obtain. This advantage makes it possible to create flood warning systems  
269 in situations where hydrographic and hydrogeological knowledge is very poor, making it very difficult to obtain additional information.  
270 Conversely, these methodologies can be applied in very complex geological and geomorphological situations (i.e., karst systems, steep  
271 slopes) where, despite the considerable knowledge of the territory, it is still impossible to build satisfactory physical models. Our case  
272 study falls precisely in this case. The Arno River basin was much studied in the past, and, in Italy, it is probably one of the most studied  
273 rivers together with the Po, the Tiber, and the Serchio. The alert model we have devised can be applied to different watercourses without  
274 having to deal with the study of the physics of the process. This makes possible to create a monitoring network for the simulation of the  
275 secondary channels as well.

276 However, this advantage can become a disadvantage if the time series is unreliable on account to the poor management of the station.  
277 Variations in the river section or a displacement of the measuring station can cause an inconsistency within the data that prevents these  
278 models from functioning correctly. This method allowed to obtain good results by exploiting an LSTM-based architecture. The errors in  
279 notification times found in this study are fully comparable with those obtained by other authors who used established physical models  
280 (Ercolani and Castelli, 2017). This comparison proved that our models are a valid tool compatible with others already used for flood  
281 forecasting. The greatest limit of our model is certainly the lack of information on the precipitation falling on the basin until the time of the  
282 forecast. If the forecast is issued before it starts raining in the basin, the model cannot predict the flood event. We think that future studies  
283 will improve these models by using precipitation forecast information extracted through artificial intelligence or physics-based techniques  
284 (physic-mathematical models, satellite image analysis). The inclusion of these techniques in the development of deep learning models can  
285 improve the prediction of a flood event.

286  
287 **Supplementary Material:** Figures 1s to 10s show some simulations performed for the 10 major events that occurred in the Arno River  
288 basin in 2019 and 2020.

289  
290 **Conflicts of Interest:** The authors declare no conflict of interest. The funders had no role in the design of the study; in the collection,  
291 analyses, or interpretation of the data; in the writing of the manuscript, or in the decision to publish the results.

292  
293 **Acknowledgements:** The authors are grateful to the Tuscan Regional Hydrologic Service for providing the data used in this work.

294 **Reference**

295 Abadi, M., Agarwal, A., Barham, P., Brevdo, E., Chen, Z., Citro, C., Corrado, G.S., Davis, A., Dean, J., Devin, M.,  
296 Ghemawat, S., Goodfellow, I., Harp, A., Irving, G., Isard, M., Jia, Y., Jozefowicz, R., Kaiser, L., Kudlur, M.,  
297 Levenberg, J., Mané, D., Monga, R., Moore, S., Murray, D., Olah, C., Schuster, M., Shlens, J., Steiner, B., Sutskever,



298 I., Talwar, K., Tucker, P., Vanhoucke, V., Vasudevan, V., Viégas, F., Vinyals, O., Warden, P., Wattenberg, M., Wicke,  
299 M., Yu, Y., Zheng, X., 2015. TensorFlow: Large-Scale Machine Learning on Heterogeneous Systems.

300 Antonetti, M., Zappa, M., 2018. How can expert knowledge increase the realism of conceptual hydrological models? A case  
301 study based on the concept of dominant runoff process in the Swiss Pre-Alps. *Hydrology and Earth System Sciences*  
302 22, 4425–4447. <https://doi.org/10.5194/hess-22-4425-2018>

303 Autorità di Bacino del Fiume Arno, 1989. PIANO DI BACINO DEL FIUME ARNO.

304 Bates, B.C. (Bryson C.), Kundzewicz, Z., Wu, S., Palutikof, J., Intergovernmental Panel on Climate Change. Working Group  
305 II, 2008. *Climate change and water*.

306 Becchi I., 1986. Introduction to the Arno basin flooding problems, in: CNR-GNDCI pubbl. (Ed.), *International Conference*  
307 *on the Arno Project*.

308 Boulmaiz, T., Guermoui, M., Boutaghane, H., 2020. Impact of training data size on the LSTM performances for rainfall–  
309 runoff modeling. *Modeling Earth Systems and Environment* 6, 2153–2164. [https://doi.org/10.1007/s40808-020-00830-](https://doi.org/10.1007/s40808-020-00830-<br/>310 w)

311 Bryndal, T., Franczak, P., Krocak, R., Cabaj, W., Kołodziej, A., 2017. The impact of extreme rainfall and flash floods on  
312 the flood risk management process and geomorphological changes in small Carpathian catchments: a case study of the  
313 Kasiniczanka river (Outer Carpathians, Poland). *Natural Hazards* 88, 95–120. [https://doi.org/10.1007/s11069-017-](https://doi.org/10.1007/s11069-017-<br/>314 2858-7)

315 Caporali, E., Rinaldi, M., Casagli, N., 2005. The Arno River Floods. *Giornale di Geologia Applicata* 1, 177–192.  
316 <https://doi.org/10.1474/GGA.2005-01.0-18.0018>

317 Chattopadhyay, A., Nabizadeh, E., Hassanzadeh, P., 2020. Analog Forecasting of Extreme- Causing Weather Patterns Using  
318 Deep Learning. *Journal of Advances in Modeling Earth Systems* 12, e2019MS001958.  
319 <https://doi.org/10.1029/2019MS001958>

320 Chollet, F., 2015. Keras.

321 Ercolani, G., Castelli, F., 2017. Variational assimilation of streamflow data in distributed flood forecasting. *Water Resources*  
322 *Research* 53, 158–183. <https://doi.org/10.1002/2016WR019208>

323 Fawaz, H.I., Forestier, G., Weber, J., Fawaz, H.I., Forestier, G., Weber, J., Idoumghar, L., Muller, P., 2020. Deep learning  
324 for time series classification : a review To cite this version : HAL Id : hal-02365025 Deep learning for time series  
325 classification : a review.

326 Gaume, E., Bain, V., Bernardara, P., Newinger, O., Barbuc, M., Bateman, A., Blaškovičová, L., Blöschl, G., Borga, M.,  
327 Dumitrescu, A., Daliakopoulos, I., Garcia, J., Irimescu, A., Kohnova, S., Koutroulis, A., Marchi, L., Matreata, S.,  
328 Medina, V., Preciso, E., Sempere-Torres, D., Stancalie, G., Szolgay, J., Tsanis, I., Velasco, D., Viglione, A., 2009. A  
329 compilation of data on European flash floods. *Journal of Hydrology* 367, 70–78.  
330 <https://doi.org/https://doi.org/10.1016/j.jhydrol.2008.12.028>

331 Gaume, E., Borga, M., LLASSAT, M.C., Maouche, S., Lang, M., DIAKAKIS, M., 2016. Mediterranean extreme floods and  
332 flash floods , in: The Mediterranean Region under Climate Change. A Scientific Update, Coll. Synthèses. IRD  
333 Editions, pp. 133–144.

334 Goodfellow, I., Bengio, Y., Courville, A., 2016. Deep Learning. MIT Press.

335 Hu, Y., Yan, L., Hang, T., Feng, J., 2020. Stream-Flow Forecasting of Small Rivers Based on LSTM.

336 IPCC, 2014. Climate Change 2014: Synthesis Report. Contribution of Working Groups I, II and III to the Fifth Assessment  
337 Report of the Intergovernmental Panel on Climate Change.

338 Jaiswal, R.K., Ali, S., Bharti, B., 2020. Comparative evaluation of conceptual and physical rainfall–runoff models. Applied  
339 Water Science 10, 48. <https://doi.org/10.1007/s13201-019-1122-6>

340 Kingma, D.P., Ba, J., 2014. Adam: A Method for Stochastic Optimization.

341 Kratzert, F., Klotz, D., Brenner, C., Schulz, K., Herrnegger, M., 2018. Rainfall – runoff modelling using Long Short-Term  
342 Memory ( LSTM ) networks 6005–6022.

343 Le, X.H., Ho, H., Lee, G., Jung, S., 2019. Application of Long Short-Term Memory (LSTM) Neural Network for Flood  
344 Forecasting. Water 11, 1387. <https://doi.org/10.3390/w11071387>

345 LeCun, Y., Bengio, Y., Hinton, G., 2015. Deep learning. Nature 521, 436–444. <https://doi.org/10.1038/nature14539>

346 Li, W., Kiaghadi, A., Dawson, C., 2020. High temporal resolution rainfall–runoff modeling using long-short-term-memory  
347 (LSTM) networks. Neural Computing and Applications. <https://doi.org/10.1007/s00521-020-05010-6>

348 Liu, D., Jiang, W., Mu, L., Wang, S., 2020. Streamflow Prediction Using Deep Learning Neural Network: Case Study of  
349 Yangtze River. IEEE Access 8, 90069–90086. <https://doi.org/10.1109/ACCESS.2020.2993874>

350 Livieris, I.E., Pintelas, E., Pintelas, P., 2020. A CNN–LSTM model for gold price time-series forecasting. Neural Computing  
351 and Applications 32, 17351–17360. <https://doi.org/10.1007/s00521-020-04867-x>

352 Luppichini, M., Favalli, M., Isola, I., Nannipieri, L., Gianecchini, R., Bini, M., 2019. Influence of topographic resolution  
353 and accuracy on hydraulic channel flow simulations: Case study of the Versilia River (Italy). Remote Sensing 11.  
354 <https://doi.org/10.3390/rs11131630>

355 Marçais, J., de Dreuzy, J.-R., 2017. Prospective Interest of Deep Learning for Hydrological Inference. Groundwater 55, 688–  
356 692. <https://doi.org/https://doi.org/10.1111/gwat.12557>

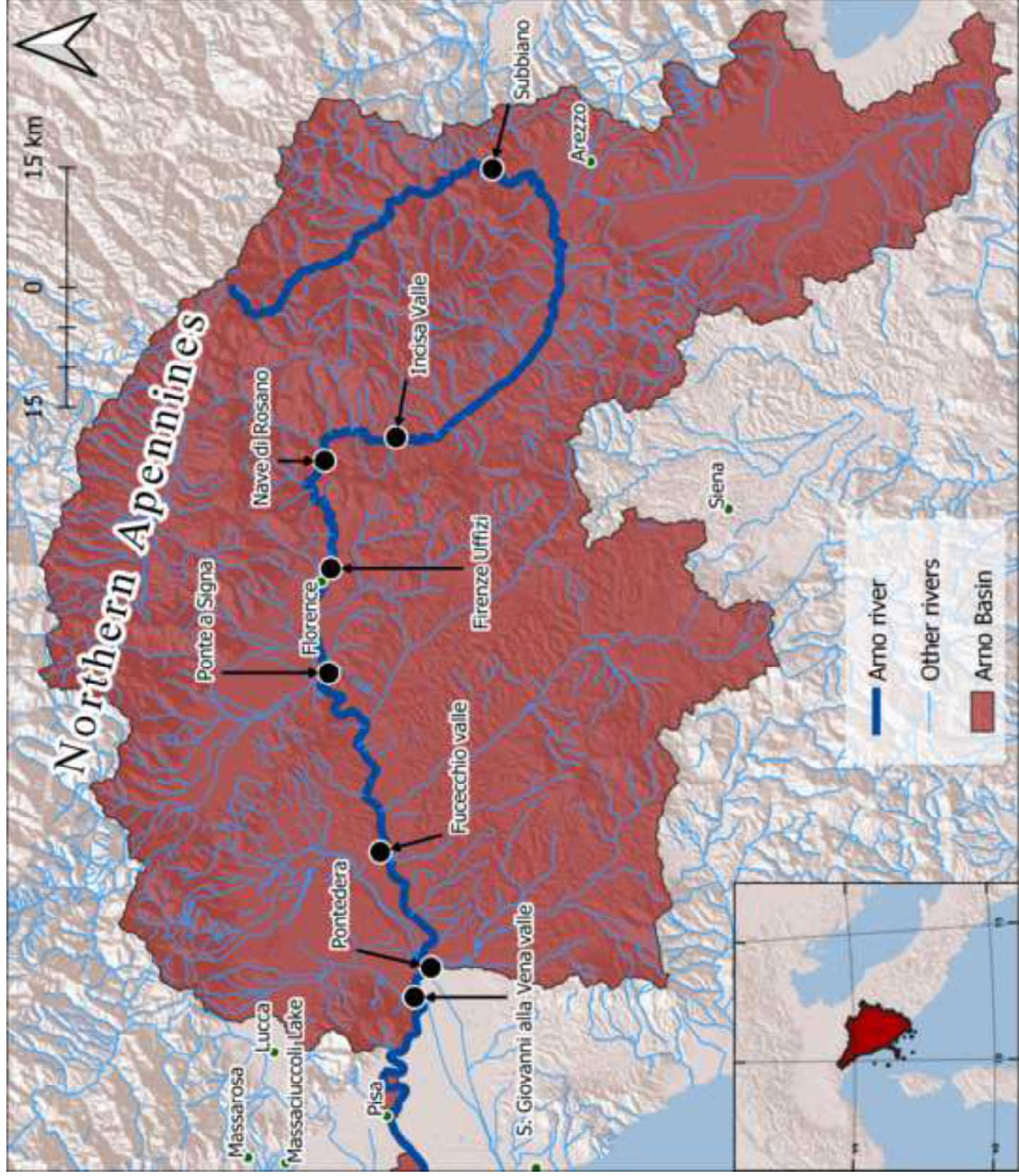
357 Nguyen, D.H., Bae, D.-H., 2020. Correcting mean areal precipitation forecasts to improve urban flooding predictions by  
358 using long short-term memory network. Journal of Hydrology 584, 124710.  
359 <https://doi.org/https://doi.org/10.1016/j.jhydrol.2020.124710>

360 Sit, M., Demiray, B.Z., Xiang, Z., Ewing, G.J., Sermet, Y., Demir, I., 2020. A comprehensive review of deep learning  
361 applications in hydrology and water resources. Water Science and Technology. <https://doi.org/10.2166/wst.2020.369>

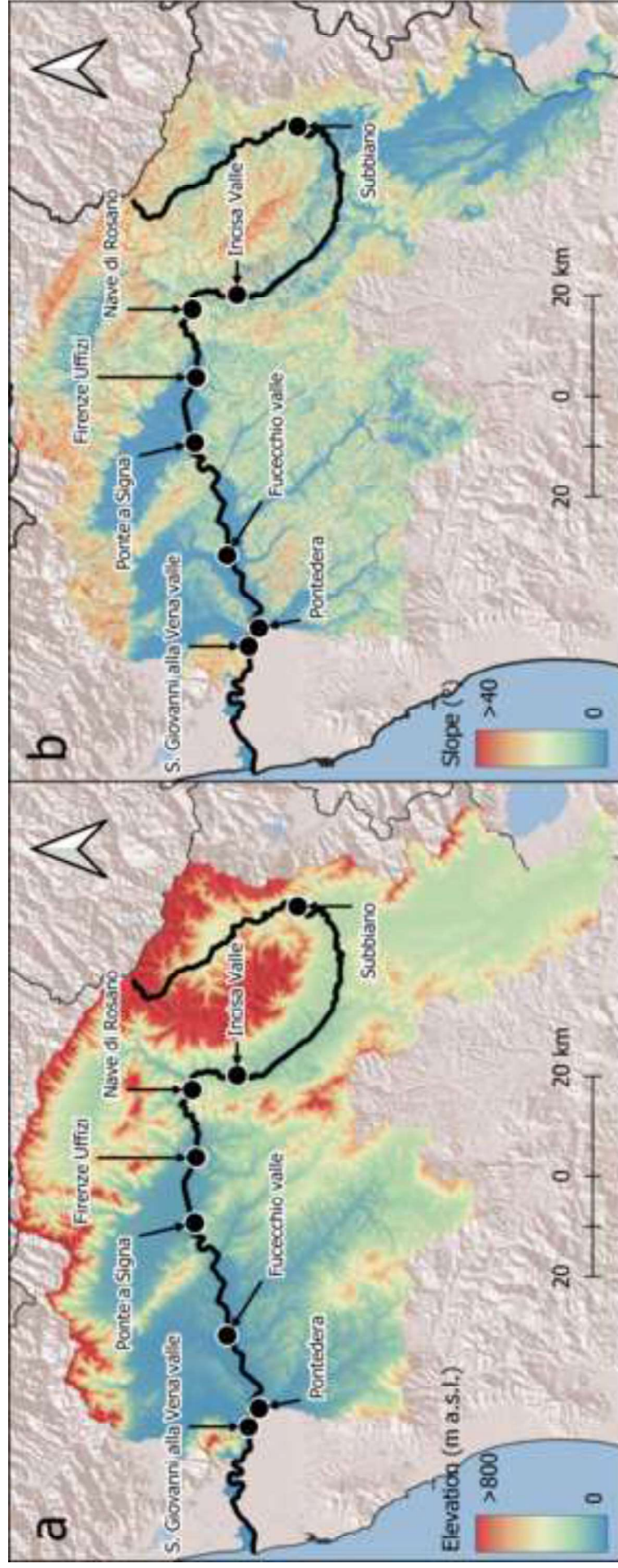
362 Sutskever, I., Vinyals, O., Le, Q. v., 2014. Sequence to Sequence Learning with Neural Networks.

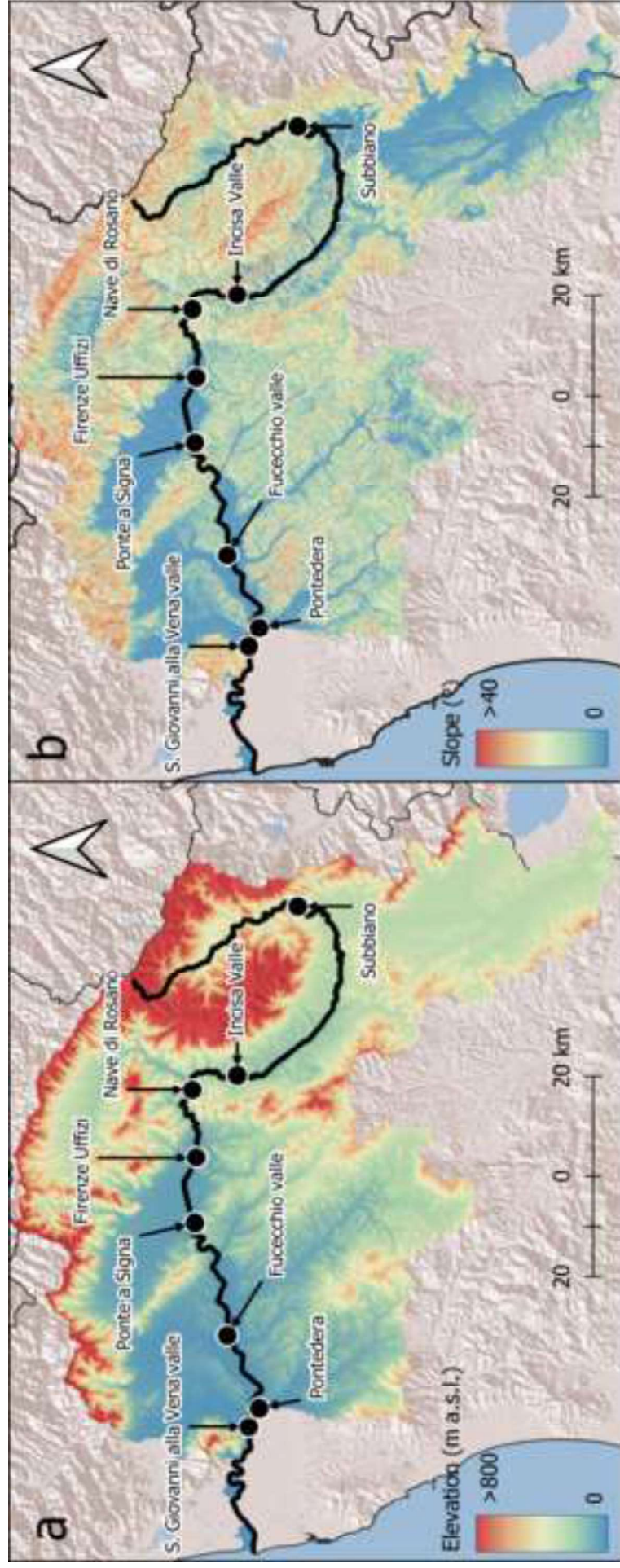
363 Tien Bui, D., Hoang, N.-D., Martínez-Álvarez, F., Ngo, P.-T.T., Hoa, P.V., Pham, T.D., Samui, P., Costache, R., 2020. A  
364 novel deep learning neural network approach for predicting flash flood susceptibility: A case study at a high frequency

365 tropical storm area. *Science of The Total Environment* 701, 134413.  
366 <https://doi.org/https://doi.org/10.1016/j.scitotenv.2019.134413>  
367 van Rossum, G., Drake, F.L., 2009. *Python 3 Reference Manual*. CreateSpace, Scotts Valley, CA.  
368 Van, S.P., Le, H.M., Thanh, D.V., Dang, T.D., Loc, H.H., Anh, D.T., 2020. Deep learning convolutional neural network in  
369 rainfall–runoff modelling. *Journal of Hydroinformatics* 22, 541–561. <https://doi.org/10.2166/hydro.2020.095>  
370 Yi, A., Li, Z., Gan, M., Zhang, Y., Yu, D., Chen, W., Ju, Y., 2019. A deep learning approach on short-term spatiotemporal  
371 distribution forecasting of dockless bike-sharing system. *Neural Computing and Applications* 31, 1–13.  
372 <https://doi.org/10.1007/s00521-018-3470-9>  
373 Zheng, J., Fu, X., Zhang, G., 2019. Research on Exchange Rate Forecasting Based on Deep Belief Network. *Neural Comput.*  
374 *Appl.* 31, 573–582. <https://doi.org/10.1007/s00521-017-3039-z>  
375



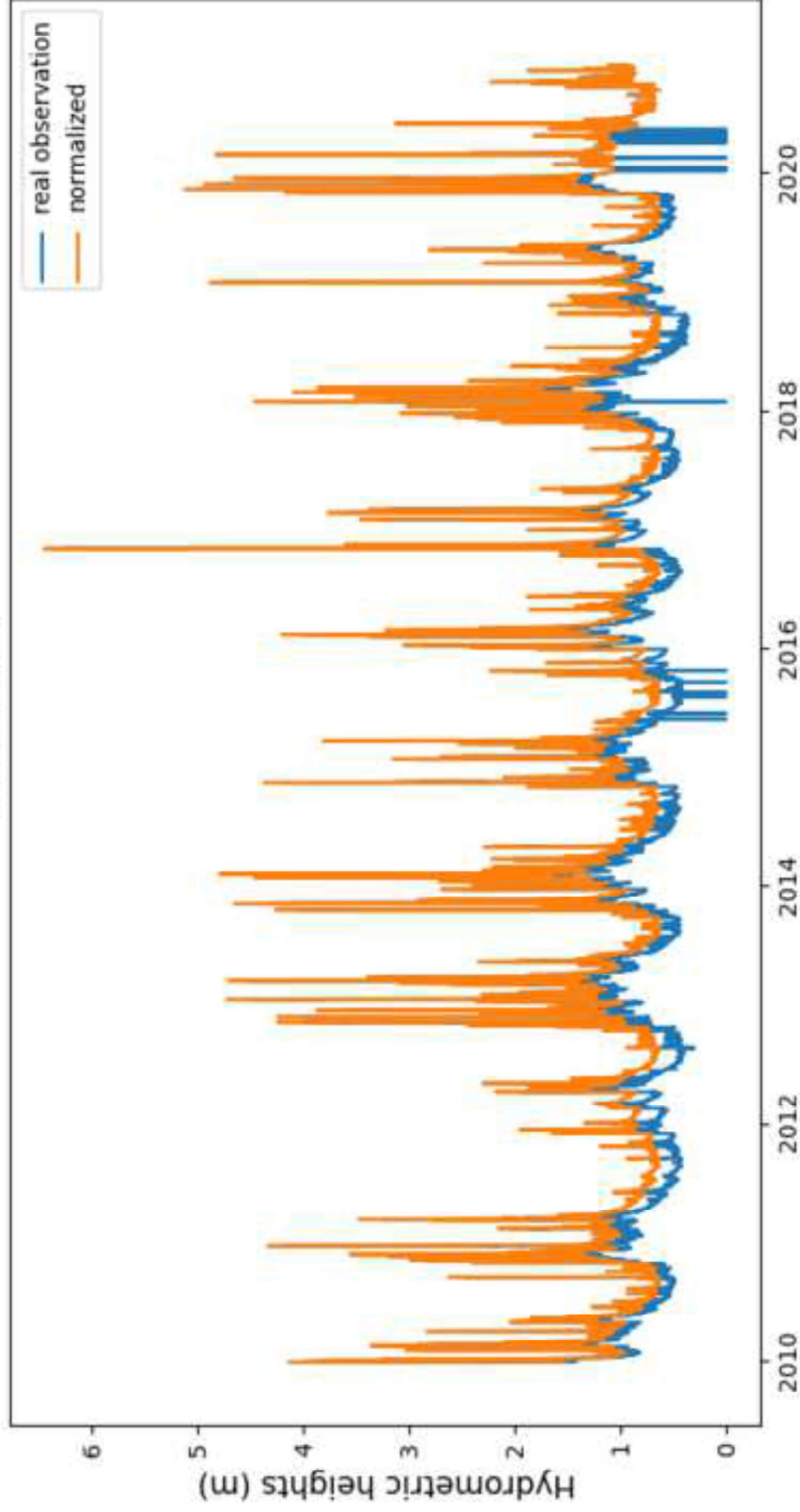


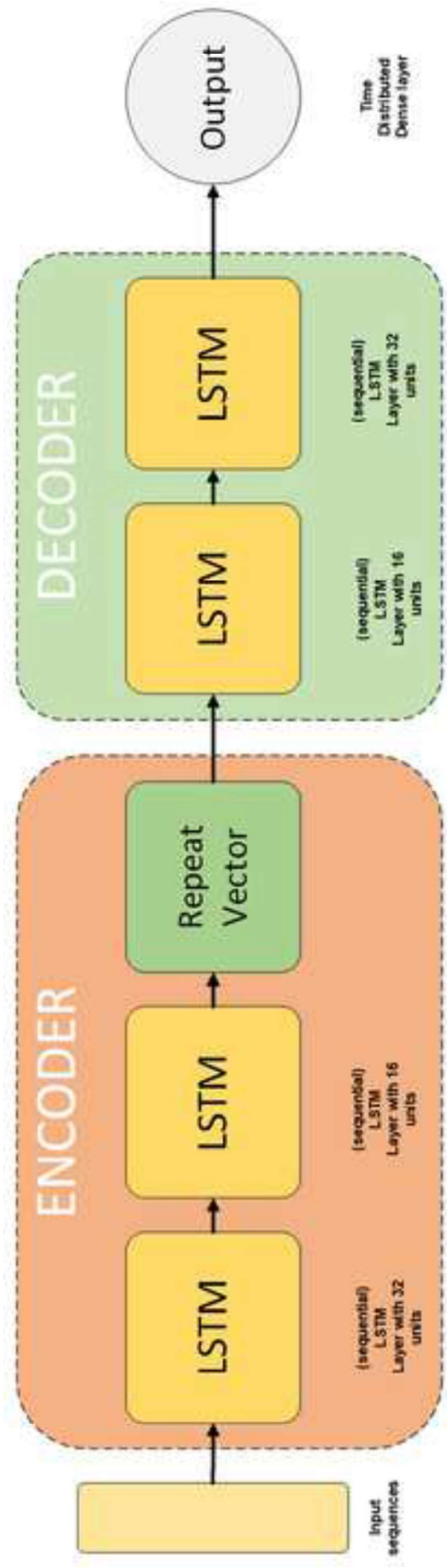


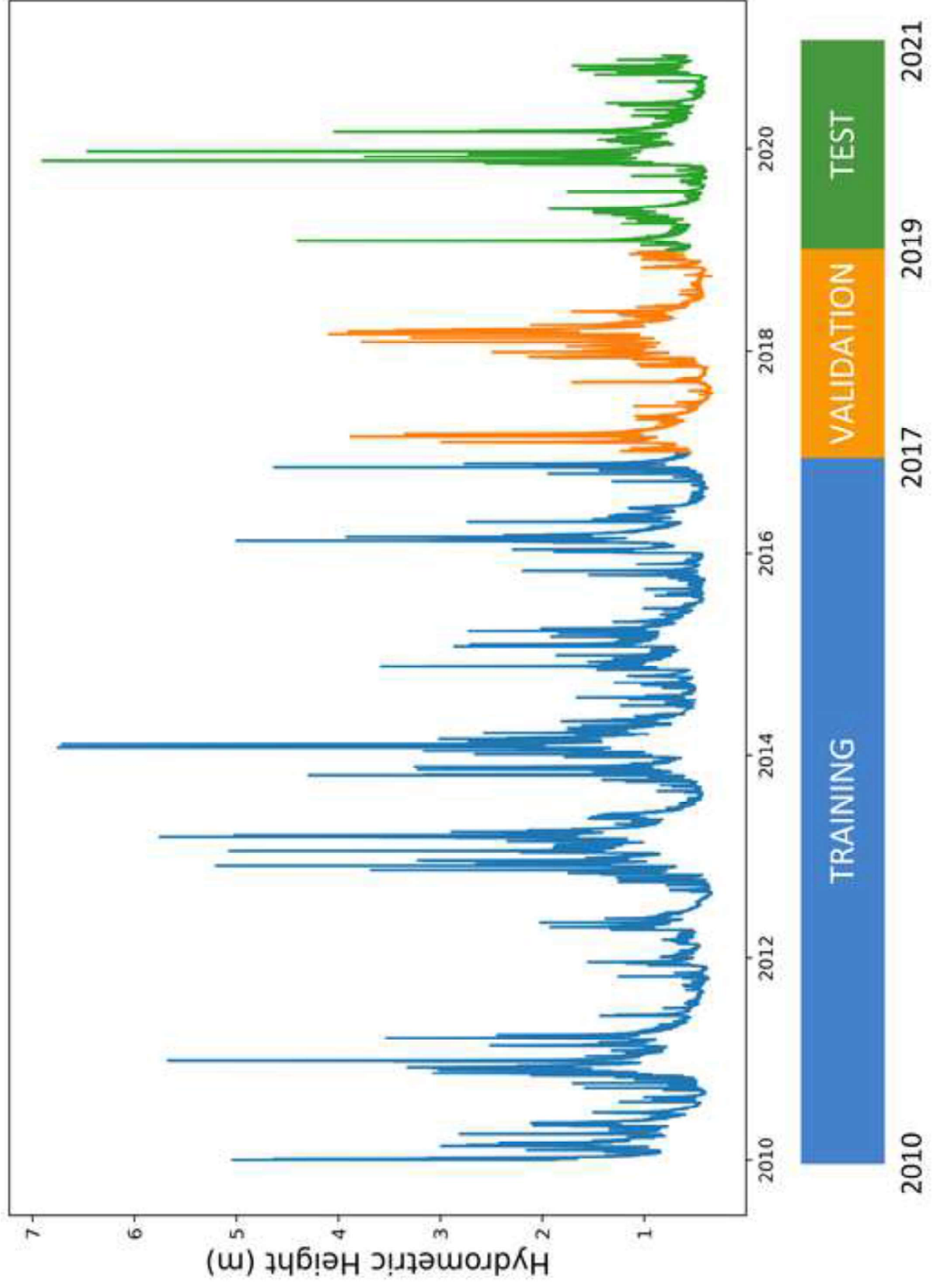


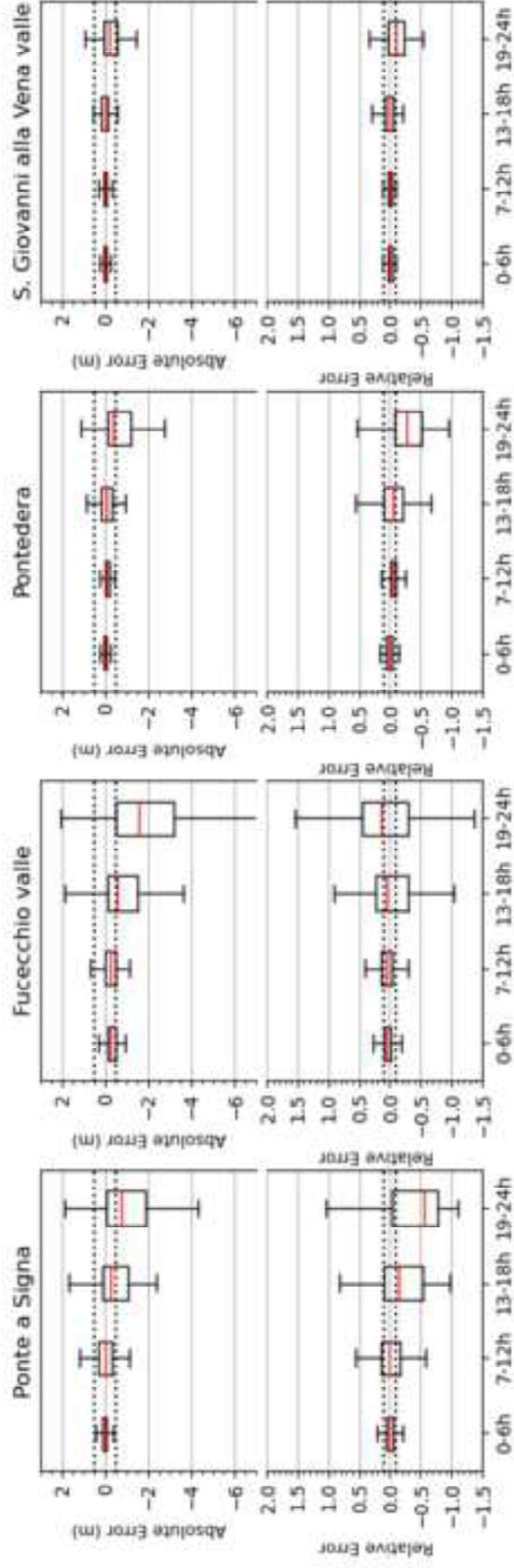
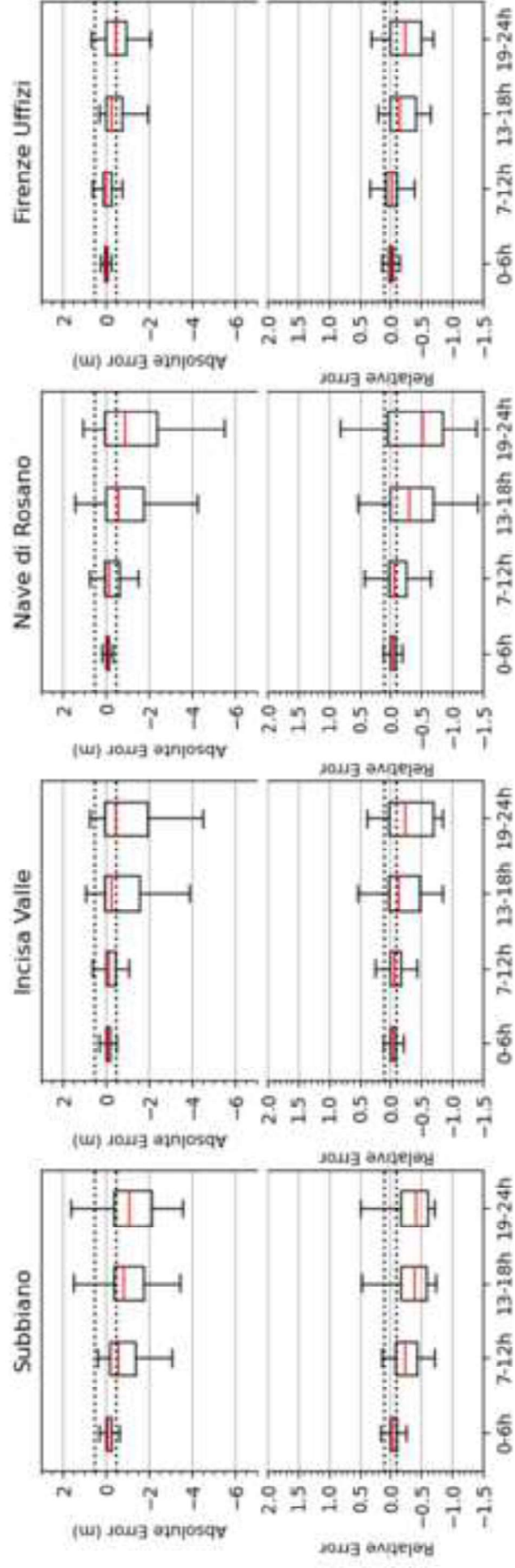


# Subbiano

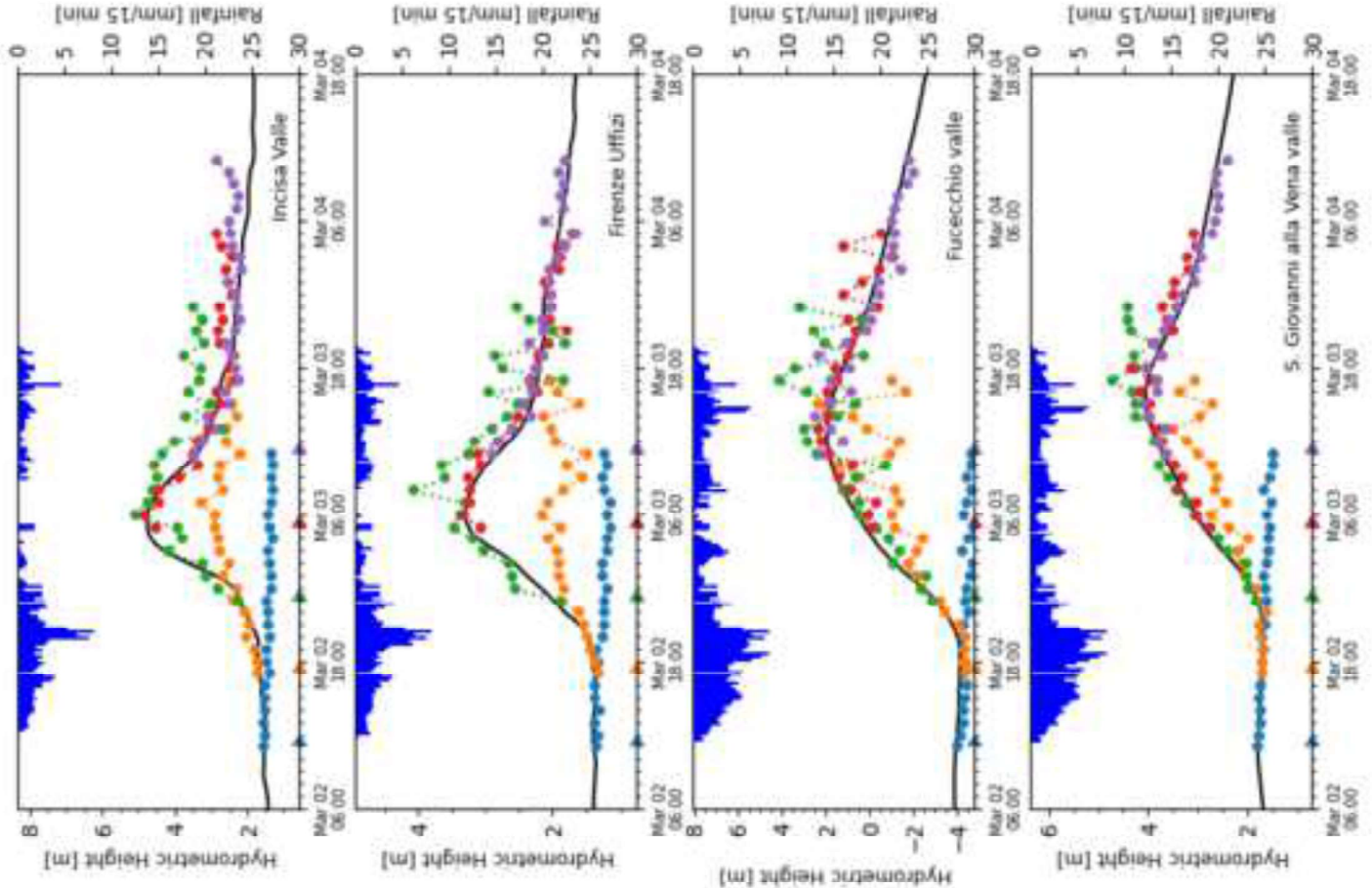
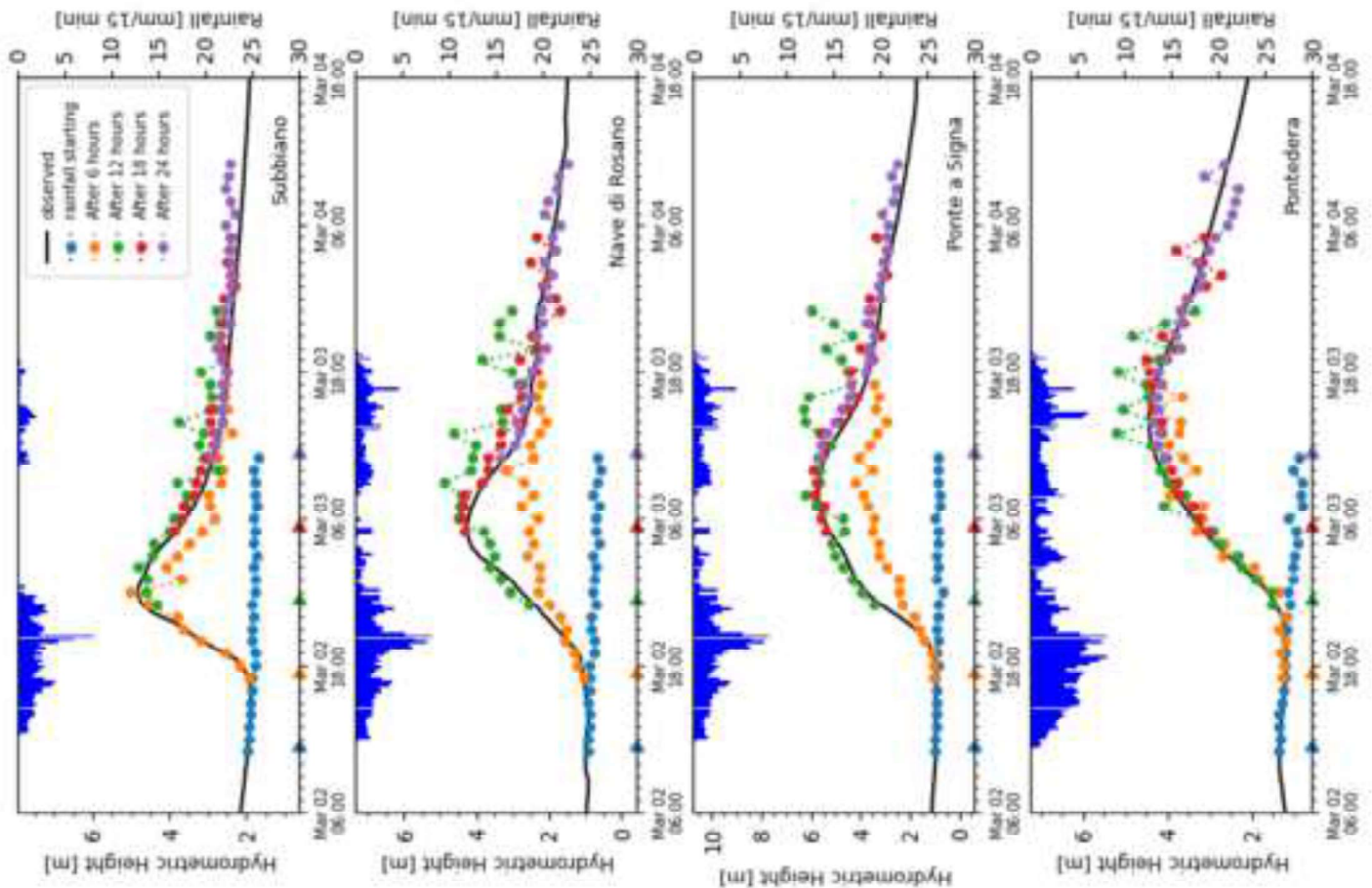


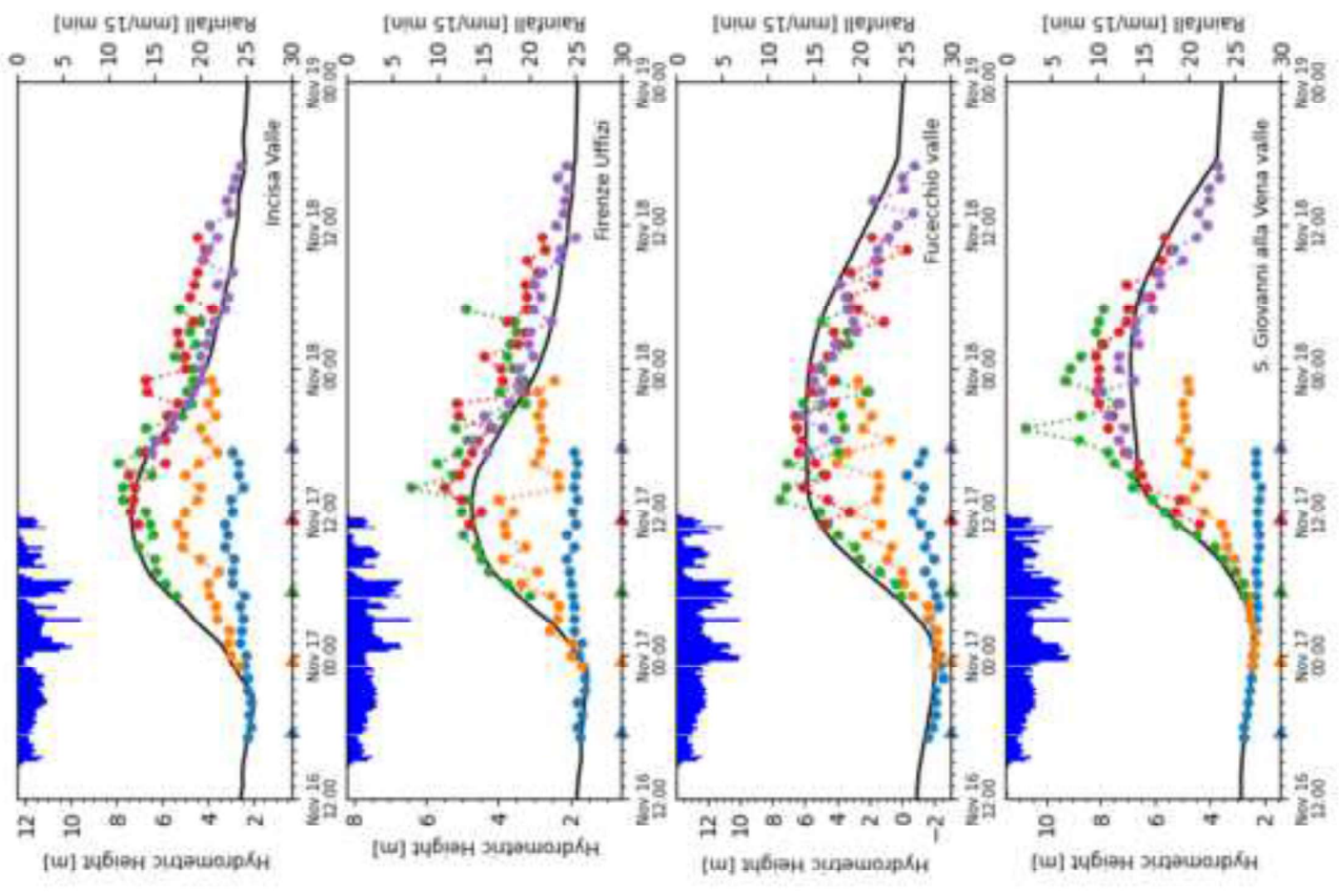
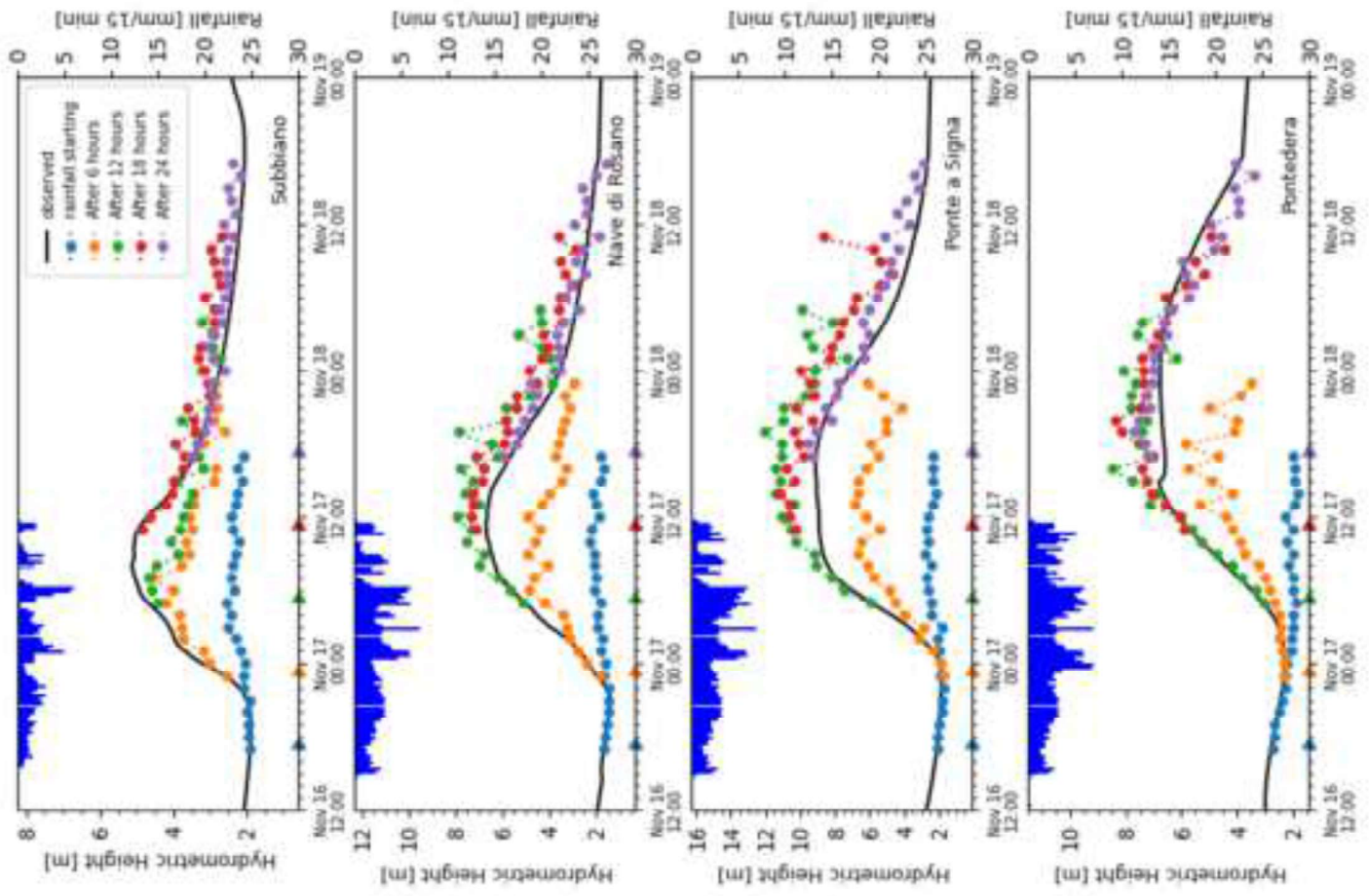
















Click here to access/download  
**Supplementary Material**  
Supplementary.docx



**Declaration of interests**

The authors declare that they have no known competing financial interests or personal relationships that could have appeared to influence the work reported in this paper.

The authors declare the following financial interests/personal relationships which may be considered as potential competing interests:

**Conflicts of Interest**

The authors declare no conflict of interest. The funders had no role in the design of the study; in the collection, analyses, or interpretation of data; in the writing of the manuscript, or in the decision to publish the results.

**Marco Luppichini:** Conceptualization, Methodology, Software, Investigation, Data curation, Writing- Original draft preparation **Michele Barsanti** Conceptualization, Methodology , Investigation, Writing- Reviewing and Editing. **Roberto Giannecchini:** Supervision, Visualization, Writing- Reviewing and Editing. **Monica Bini:** Supervision, Writing- Reviewing and Editing, Conceptualization